Analytical and Bioanalytical Chemistry (2021) 413:6793–6802
https://doi.org/10.1007/s00216-021-03273-z

RESEARCH PAPER

Quantitative measurements of free and immobilized *Rg*DAAO Michaelis-Menten constant using an electrochemical assay reveal the impact of covalent cross-linking on substrate specificity

Siba Moussa[1] · Danny Chhin[1] · Loredano Pollegioni[2] · Janine Mauzeroll[1]

Received: 20 January 2021 / Revised: 22 February 2021 / Accepted: 3 March 2021 / Published online: 1 April 2021

Abstract

Challenges facing enzyme-based electrochemical sensors include substrate specificity, batch to batch reproducibility, and lack of quantitative metrics related to the effect of enzyme immobilization. We present a quick, simple, and general approach for measuring the effect of immobilization and cross-linking on enzyme activity and substrate specificity. The method can be generalized for electrochemical biosensors using an enzyme that releases hydrogen peroxide during its catalytic cycle. Using as proof of concept *Rg*DAAO-based electrochemical biosensors, we found that the Michaelis-Menten constant (K_m) decreases post immobilization, hinting at alterations in the enzyme kinetic properties and thus substrate specificity. We confirm the decrease in K_m electrochemically by characterizing the substrate specificity of the immobilized *Rg*DAAO using chronoamperometry. Our results demonstrate that enzyme immobilization affects enzyme substrate specificity and this must be carefully evaluated during biosensor development.

Keywords Microelectrodes · Enzymes · Activity · Crosslinker · D-Serine

Introduction

Enzyme immobilization on solid supports is a cost reduction technique that has been widely adopted in biosensing [1–7] and biocatalysis [8–10]. Yet, the catalytic performance of an immobilized enzyme will change based on the chosen method, i.e., nature of the substrate, enzyme loading, and concentration [11–14]. For biosensors based on redox-active enzymes, there are established quantitative analytical expressions to evaluate the enzyme activity but they do not apply to non-redox enzymes [15–19]. Techniques such as AFM [20], SECM [21–23], SEM [24], and FTIR [25, 26], employed to characterize non-redox enzymatic biosensors, are neither quantitative nor representative of the final device structure. There is no simple and analytically valid method to quantify the activity of immobilized non-redox enzymes. Thus, it is difficult to compare performance between different biosensor designs and fabrication methods.

Traditionally, enzymes are immobilized through a range of methods [27]. The key immobilization methods are either chemical (i.e., covalent attachment and cross-linking) or physical (i.e., adsorption and entrapment) [28]. Depending on their application, which ranges from the pharmaceuticals to the cosmetic industries, support materials for enzyme immobilization are either organic (i.e., natural or synthetic polymers) or inorganic (i.e., silica and glass) based [28–30]. Both support type and immobilization impact enzyme stability, a desired property for enzyme industrial application. Covalent-based enzyme immobilization is the most commonly used technique due to the resulting high enzyme stability. It is based on chemical linker functional group reactivity with reactive residues of the enzymes, such as amino groups, to form stable bonds which impact enzyme conformation, giving rise increased enzyme stability [31]. In addition to enzyme stability, enzyme activity is an important parameter in assessing enzyme performance. Studies using optical oxygen assays and electrospray

Published in the topical collection *Electrochemistry for Neurochemical Analysis* with guest editors Ashley E. Ross and Alexander G. Zestos.

✉ Janine Mauzeroll
Janine.mauzeroll@mcgill.ca

[1] Department of Chemistry, McGill University, 801 Sherbrooke Street West, Montreal, Quebec H3A 0B8, Canada

[2] Dipartimento di Biotecnologie e Scienze della Vita, Università degli studi dell'Insubria, via J. H. Dunant 3, 21100 Varese, Italy

ionization-mass spectrometry have shown that immobilization may either reduce [32], maintain [33, 34], or improve enzyme activity [35].

Herein, we propose to immobilize an enzyme to the surface of a poly-m-phenylenediamine modified microelectrode (PPD-ME) and measure the chronoamperometric current of the enzyme electroactive byproduct to quantify its catalytic activity. As a proof of concept, the microelectrode-based electrochemical characterization approach (MECA) is applied to yeast D-amino acid oxidase (*Rg*DAAO), which has significant potential for applications as a D-amino acid detecting biosensor [21, 36–39].

*Rg*DAAO is involved in the degradation of D-amino acids such as D-serine [40], which regulates neurotransmission in the central nervous system. Hence, changes in DAAO function and D-amino acid levels are linked to the onset of chronic diseases such as depression, schizophrenia, Alzheimer's, and gut inflammation [41–43]. Biosensors are simple, low-cost tools that allow for real-time analyte detection: employing *Rg*DAAO biosensors is an attractive approach for probing D-amino acids [44, 45]. Furthermore, in oxidase enzymes like *Rg*DAAO, the electroactive enzyme catalysis byproduct is hydrogen peroxide (H_2O_2), which is oxidizable at platinum ME surfaces [45–47]. As such, the MECA method is applicable to enzymes producing an electroactive product.

In this work, MECA is used to measure the kinetics for both free and ME-immobilized *Rg*DAAO. The Michaelis-Menten constant (K_m) obtained using MECA is compared to spectrophotometric assays for free *Rg*DAAO and the Shu and Wilson method for immobilized *Rg*DAAO. The MECA was also applied to study *Rg*DAAO substrate specificity. Finally, we build on these findings by discussing the effect of the presence of dual substrates (D-alanine and D-serine) on *Rg*DAAO biosensor response.

Experimental section

Chemicals D-Serine (99%), D-alanine (99%), D-aspartate (99%), glycine (≥98.5%), m-phenylenediamine flakes (99%), bovine serum albumin (BSA, ≥98%), glycerol (≥99), o-dianisidine (o-DNS), H_2O_2 (30% vol/vol in H_2O), and 2-mercaptoethanol were all purchased from Sigma-Aldrich. Glutaraldehyde (50% in H_2O) was purchased from Fischer Scientific.

Enzyme purification and expression Recombinant *Rg*DAAO wild type (WT) was prepared as reported in the literature [48]. Briefly, recombinant *Rg*DAAO WT was expressed in BL21(DE3)pLysS *E. coli* cells using the pT7-HisDAAO expression vector and purified by HiTrap Chelating chromatography (GE Healthcare Bio-sciences). The final preparation of *Rg*DAAO WT was stored in 20 mM Tris-HCl (pH 8.0), 100 mM NaCl, 10% v/v glycerol, and 5 mM 2-mercaptoethanol. The enzyme purity was confirmed by SDS-PAGE. The final enzyme solution was concentrated to 56.8 mg mL^{-1} protein in 0.01 M phosphate-buffered saline (PBS, pH 7.4) containing 1% v/v glycerol and 25 mg mL^{-1} BSA.

Spectrophotometric characterization of *Rg*DAAO$_{free}$ Hydrogen peroxide production was detected using a coupled enzyme *o*-DNS activity assay as discussed in the literature [49]. Briefly, hydrogen peroxide produced from the enzymatic reaction is reduced by horseradish peroxidase that simultaneously oxidizes *o*-DNS to give a colored compound with an absorption maxima at 440 nm. To explore pH effects on the specific activity of *Rg*DAAO$_{free}$, activity assays were carried out in both 100 mM sodium pyrophosphate (NaPPi, pH = 8.5) and 100 mM potassium phosphate (KPi, pH = 7.4) with various substrates (D-serine, D-alanine, and glycine). One unit of enzyme is defined as the amount of enzyme that converts 1 μmol of substrate per minute at 25 °C [50].

PPE-ME and *Rg*DAAO-PPD-ME preparation Platinum (Pt) disk MEs (10 μm) were prepared according to the literature [51]. Briefly, a soda-lime glass capillary was pulled and a Pt wire was inserted into the capillary, which was then sealed. The ME was polished until the Pt wire was exposed, revealing a disk-shaped surface geometry. This was followed by rinsing the ME with Millipore MilliQ water (18.2 MΩ·cm), 70% ethanol, and acetone. The R_g, defined as the glass sheath to the exposed platinum diameter ratio, was confirmed with optical microscopy using a customized Axio Vert.A1 inverted microscope (Zeiss, Oberkochen, Germany). The R_g was 5 for all MEs. A permselective polymer was then electrodeposited on the microelectrode surface using cyclic voltammetry (0 to +1000 mV, 5 cycles) with 0.1 M m-phenylenediamine (PPD) prepared in 0.01 M PBS (pH = 7.4) [44].

To fabricate the full biosensor, 2 μL of the enzyme (56.8 mg mL^{-1} in 25 mg mL^{-1} BSA) was drop-casted onto a polydimethylsiloxane-coated glass slide. This was done to ensure hydrophobicity of the surface, which facilitated enzyme deposition onto the PPD-ME tip. The PPD-ME was immersed in the enzyme droplet for 5 s and then removed to dry for 4 min. The immersion process was repeated four times until a small amount of enzyme had adsorbed onto the PPD-ME, confirmed with optical microscopy. Glutaraldehyde vapor-based cross-linking of the PPD layer with the enzyme layer was achieved by placing the biosensor in a sealed chamber containing 10 mL of glutaraldehyde solution (50% v/v in H_2O) for 10 min.

Electrochemical measurements For chronoamperometry, the biosensor was biased at 0.5 mV vs. Ag/AgCl was performed using an Electrochemical Probe Scanner 3 (HEKA Elektronik, Lambrecht, Germany). All potentials were recorded relative to a chloridized silver wire (fabricated in-house, radius = 0.250 mm) quasi-reference electrode [51]. All solutions were prepared in phosphate-buffered saline (PBS, 0.01 M, pH 7.4).

Similarly, cyclic voltammetry experiments using the $RgDAAO_{immob}$-PPD-ME (biosensor) immersed in individual solutions of D-serine and D-alanine were performed (−0.1 to 0.6 V vs. Ag/AgCl wire, 0.1 $V \cdot s^{-1}$).

Electrochemical characterization of $RgDAAO_{free}$ and $RgDAAO_{immob}$ H_2O_2 production from free *Rg*DAAO reaction with D-serine using a PPD-ME was measured to assess $RgDAAO_{free}$ activity. *Rg*DAAO was thawed on ice and then warmed to room temperature for 5 min. An oxidative potential step of 0.5 V vs. Ag/AgCl was applied to a solution of 200 μL of D-serine (0.01 M PBS, pH = 7.4); then, 1 μL of *Rg*DAAO (56.8 $mg \cdot mL^{-1}$) was added during mixing. The increase in current following the addition of *Rg*DAAO was used to calculate the specific activity of *Rg*DAAO towards D-serine at a given concentration.

To study the effect of enzyme immobilization on the biosensor specific activity, the current response from a biosensor was measured using a potential step of 0.5 V vs. Ag/AgCl in D-serine solutions (0.01 M PBS, pH = 7.4) at different concentrations.

Numerical simulations A 2D axisymmetric model was built using COMSOL Multiphysics version 5.3a was used to simulate the steady-state current following the oxidation of H_2O_2 at the ME tip. A parametric sweep was applied to determine the current value (i) at various concentrations to generate a calibration curve for the *Rg*DAAO-PPD-ME with D-serine. The diffusion coefficient (D_{app}) was also parametrized to determine the apparent diffusion coefficient of H_2O_2 through the PPD layer. Following the minimization of the sum of squared residuals between the simulated and experimental calibration curve data, the diffusion coefficient was extracted. To ensure that both calibration curves were similar, the slopes of the regression lines were compared with a two-tailed Student's t-test ($t(4) = 0.27$, $p = .800$) (see Supplementary Information (ESM) for full model details).

Data analysis All experimental data presented are the mean of triplicate measurements unless otherwise stated. Error bars represent standard deviation (±S.D.) unless otherwise stated. A two-tailed Student's t-test was used for statistical testing ($\alpha = 0.05$). Data were analyzed and treated on Matlab R2016b (Mathworks, Natick, USA). Kinetic curves were built using an in-house developed code on Matlab R2016b (see ESM for full code details). All other data were imported into Rx64 3.5.2 (Windows version) for visualization. All electrochemical currents were normalized by the blank signal.

Results and discussion

Developing an electrochemical method to probe kinetics of redox molecule formation from immobilized enzyme catalysis

For neutral and basic D-amino acids, *Rg*DAAO's reaction produces H_2O_2, ammonia, and α-keto acid (Fig. 1) [49]. The rate of product formation is typically determined using spectrophotometric methods, i.e., *o*-DNS assays where absorbance changes are measured corresponding to enzymatic H_2O_2 production (Fig. 1a). However, they have limited sensitivity, are prone to optical interferences (such as solution turbidity) [52], and cannot be applied to immobilized enzymes.

Alternatively, *Rg*DAAO oxygen consumption can be measured with electrochemical assays (Fig. 1b). Electrochemical oxygen consumption assays do not suffer from spectrophotometric method disadvantages. Yet, oxygen consumption assays do not quantify H_2O_2 product formation, require a specific device, and do not represent the final biosensor device architecture [49].

The proposed MECA approach (Fig. 1c) enables direct measurement of redox-active molecules formed from immobilized enzyme catalysis, an approach free of optical interferences. Using amperometric PPD-modified MEs, the MECA measures the reagent-free enzymatic rate of H_2O_2 formation. Direct enzyme activity quantification is achieved by

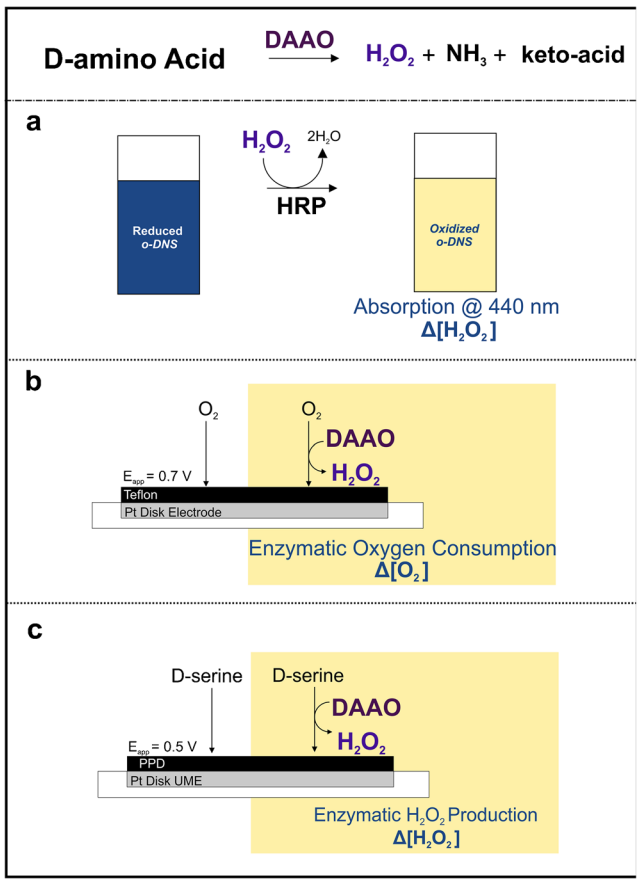

Fig. 1 The **a** spectrophotometric, **b** electrochemical, and **c** proposed MECA method used to determine the activity of the $RgDAOO_{free}$ and $RgDAAO_{immob}$ form of the enzymes. The MECA method directly quantifies H_2O_2 production

measuring the rate of current change ($\frac{di}{dt}$) from H_2O_2 oxidizing under a fixed potential (0.5 V vs. Ag/AgCl) (Fig. 1c).

Analytical equations for H_2O_2 detection at the ME surface Under diffusion limited regimes ($V \geq 0.5$ V vs. Ag/AgCl), the H_2O_2 oxidative steady-state current (i) at a disk ME is defined by [53]:

$$i = \beta(R_g)4nFaD_{app}C \quad (1)$$

where $\beta(R_g)$ is a parameter associated with the R_g of the disk ME ($\beta(R_g)$ =1.04 for R_g = 5) [54], n is the number of electrons involved in the rate-determining reaction, F is Faraday's number, C is the H_2O_2 concentration (M), D_{app} is the apparent H_2O_2 diffusion coefficient towards the electroactive ME surface, and a is the radius of the electroactive area (m). Optical microscopy is used to evaluate a and β.

Using the relationship between concentration and current measured at the microelectrode surface, the rate of H_2O_2 detection ($dC_{H_2} \frac{O_2}{dt}$) is as follows:

$$\frac{dC_{H_2O_2}}{dt} = \frac{di}{dt}\frac{1}{4nFD_{app}\beta(R_g)a} \quad (2)$$

Accounting for the presence of a permeable polymer layer at the ME surface in H_2O_2 detection To solve for $dC_{H_2} \frac{O_2}{dt}$, an approximation of the apparent H_2O_2 diffusion coefficient, D_{app} is required. Due to the presence of a permeable PPD layer at the Pt surface, transport across the PPD layer must be considered in the D_{app} value. To extract D_{app} corresponding to H_2O_2 diffusion from the bulk through the PPD and towards the ME surface, a numerical model in COMSOL Multiphysics was built to generate simulated calibration curves at various D_{app} values (see SI for full model details). Next, the simulated calibration curves were fit to experimental calibration curves.

The experimental calibration was generated by extracting i_{ss} from the oxidation current profile for H_2O_2 produced by the *Rg*DAAO reaction with 0–25 μM D-serine (ESM Fig. S2). This concentration range is relevant to D-serine levels in brain extracellular spinal fluid (0–10 μM) from quantification studies performed in human and animal models [36, 44, 55, 56].

Contribution of enzyme kinetics towards H_2O_2 detection Enzyme kinetics play a dominating role in H_2O_2 detection at the PPD-modified ME surface. To demonstrate that the signal detected at the ME surface is associated with enzymatic H_2O_2 production, a calibration curve of the PPD-ME immersed in H_2O_2 solutions was generated. The PPD-ME calibration curve was compared to calibration curves of the biosensor immersed in D-serine solutions. The two different calibrations showed good agreement with one another (ESM Fig. S2). As such, the electrochemical enzyme activity (EA) in μmol min^{-1} mL^{-1} can be related to the H_2O_2 current at the PPD-ME (Eq. 2). The enzyme reaction-dependent increase in H_2O_2 production is proportional to the current transient measured at the ME surface.

To compare *Rg*DAAO$_{free}$ and *Rg*DAAO$_{immob}$, the EA values are normalized by the enzyme concentration (mg_{DAAO}/mL), total solution volume (mL_{total}), and enzyme volume used for the assay (mL_{DAAO}). Normalization yields the specific electrochemical activity (SEA) expressed as U/mg_{DAAO} as follows:

$$\text{SEA} = \frac{U}{mg_{DAAO}} = \text{EA} \times \frac{mL_{total}}{mL_{DAAO}} \times \frac{mL}{mg_{DAAO}} \quad (3)$$

***K_m* values are determined with the MECA method for *Rg*DAAO$_{free}$ and RgDAAO$_{immob}$** To determine the SEA at different D-serine concentrations, the current transient ($\frac{di}{dt}$) was calculated from chronoamperograms. Using a PPD-ME immersed in D-serine solutions ranging from 0.1 to 25 mM, chronoamperograms were recorded at 0.5 V vs. Ag/AgCl for each concentration (Fig. 2a). The initial current transient at D-serine concentrations lower than 0.1 mM was not used due to the PPD-ME response time and instrument resolution. In the first 400 s, a background current was recorded. At 400 s, the addition of *Rg*DAAO$_{free}$ under solution mixing led to the observed current transient from H_2O_2 production. Time-dependent current changes in the initial linear range (30 s) of the *Rg*DAAO$_{free}$ reaction were used to determine SEA values at each D-serine concentration. By fitting SEA values to the Michaelis-Menten equation using a non-linear least squares regression hyperbolic model (Fig. 2b), the K_m for D-serine of *Rg*DAAO$_{free}$ is calculated (Eq. 4).

$$\text{SEA} = \frac{\text{SEA}_{max}[S]}{K_m + [S]} \quad (4)$$

Similarly, the SEA for *Rg*DAAO$_{immob}$ was determined. Briefly, a biosensor poised at 0.5 V vs. Ag/AgCl was immersed in a solution of PBS for 300 s where a background current was observed. At 300 s, a standard D-serine solution (0–25 mM) replaced the PBS solution, where mixing resulted in several current transients. An increase in H_2O_2 oxidation current is observed upon D-serine addition (Fig. 2c). The first 15 s of the linear portion of the current profile of the *Rg*DAAO$_{immob}$ reaction was used to calculate $\frac{di}{dt}$. Using a modified version of Eq. (3) where $mL_{total}/mL_{DAAO} = 1$, EA was normalized to the concentration of enzyme immobilized on the PPD-ME surface (56.8 mg/mL). Then, individual SEA values were fit to a Michaelis-Menten model (Fig. 2b). For

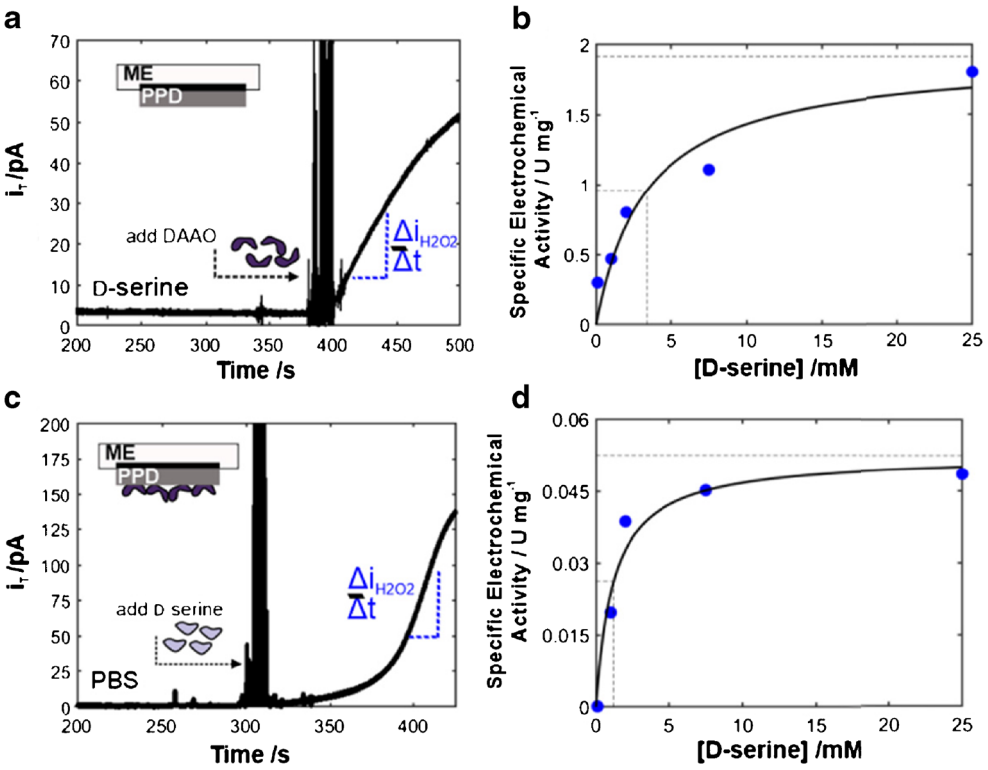

Fig. 2 **a** Schematic of experiment (in 25 mM D-serine) used to build the MM curve for the *Rg*DAAO$_{free}$. **b** MM curve used to determine K_m value for the free *Rg*DAAO$_{free}$ (3.69 mM). **c** Schematic of experiment used to build the MM curve for the immobilized enzyme. **d** MM curve used to determine K_M value for *Rg*DAAO$_{immob}$ (1.21 mM)

fitting the data points to a Michaelis-Menten model, we recommend using a minimum of four data points. However, to improve the fit of a Michaelis-Menten model, we recommend using nine data points over a wide range of substrate concentrations.

From the Michaelis-Menten model fit, the *Rg*DAAO$_{immob}$ K_m value obtained by MECA (Fig. 2b, d) is 3-fold lower than that of *Rg*DAAO$_{free}$, suggesting an increase in apparent D-serine affinity. From the MM curves in Fig. 2, both *Rg*DAAO forms exhibit substrate saturation at 25 mM. Moreover, cyclic voltammograms (CVs) of the biosensor in D-serine and D-alanine solutions show changes in substrate selectivity as a function of substrate concentration for *Rg*DAAO$_{immob}$ (ESM Fig. S3). Both results suggest the possibility of tuning the enzyme's substrate specificity through immobilization as previously demonstrated for other enzymes such as lipase [57] and ester hydrolase [58]. Substrate specificity changes are tied to the cross-linker nature which affects enzyme orientation, substrate access to the enzyme active site, and the altered surface chemistry of the support matrix [59].

While the MECA does not determine all enzyme kinetic parameters, it is suitable for comparisons of surface-immobilized enzymes unlike conventional methods such as spectrophotometric assays. The MECA is applicable for biosensors where an electroactive product is probed. For practical MECA application, we recommend consistency in enzyme concentrations for immobilization: this enables valid comparisons across biosensor design strategies.

Validation of the MECA method To determine the validity of MECA, its results were compared against established methods namely the standard *o*-DNS spectrophotometric assay [49] and an electrochemical method, defined in this work as the Shu and Wilson method [36, 60–62]. The Shu and Wilson method (Eq. 5), derived for the rotating enzyme disk electrode, has been applied in the past as an analytical method to determine the K_m value for electrode surf immobilized enzymes [7, 36, 60, 63, 64]. This method uses steady-state current measurements for analysis and is usually applied only for surface bound enzymes. Spectrophotometric assays, on the other hand, use rates of absorbance changes and are typically employed with free enzymes.

The Shu and Wilson method is based on the theory of Levich rotating disk electrodes [60]. The method demonstrates that the Levich electrode equation is consistent with the steady-state current trend of amperometric enzyme electrodes. Chronoamperometry is used to extract i_{ss} corresponding to H_2O_2 oxidation at different substrate concentrations. The K_m is calculated using the measured i_{ss} for each D-serine concentration as follows [65, 66]:

$$i_{ss} = \frac{i_{max}[S]}{K_m + [S]} \quad (5)$$

where i_{max} is the maximum H_2O_2 oxidative current at substrate saturating conditions and $[S]$ is the substrate concentration.

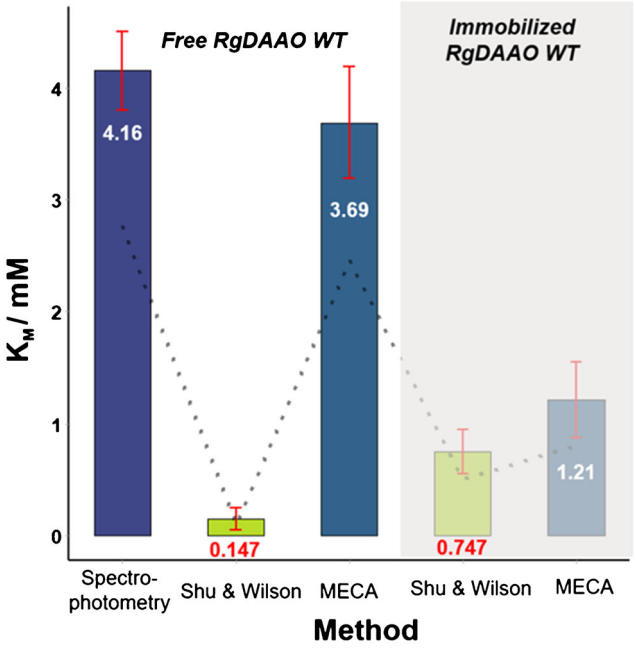

Fig. 3 K_m values derived from non-linear least squares fit of the individual activity values using the spectrophotometric assay, the Shu and Wilson method, and the MECA approach for both the free and immobilized *Rg*DAAO$_{free}$ and RgDAAO$_{immob}$ WT at pH = 7.4

For *Rg*DAAO$_{free}$, the Shu and Wilson method underestimate the K_m by a factor of ~30 compared to the spectrophotometric method (Fig. 3). In comparison, the MECA approach underestimates the K_m by a factor of ~0.12. The difference between the spectrophotometric and MECA derived K_m is ascribed to the rejection of approximately 80% of the produced H_2O_2 by the permselective PPD layer: the PPD layer induces hindered diffusion towards electroactive ME surface [21]. This hindered diffusion masks the original rate of H_2O_2 production, causing a deviation in matching the K_m determined with spectrophotometry. For *Rg*DAAO$_{immob}$, the K_m value is lower than for *Rg*DAAO$_{free}$ for both the MECA and Shu and Wilson methods (Fig. 3). Moreover, when comparing MECA to the Shu and Wilson method, the latter method gave a lower K_m value for *Rg*DAAO$_{immob}$ suggesting that the Shu and Wilson method also underestimates this kinetic parameter.

Using the MECA, the *Rg*DAAO$_{immob}$ K_m value (1.21 mM) is less than the *Rg*DAAO$_{free}$ K_m (3.69 mM). The change in the K_m is due to alterations in the rate of enzyme catalysis (k_{cat}) and/or dissociation (K_d) as both impact the overall K_m value [67]. Variations in K_m values for the same enzyme represent changes in enzyme substrate specificity.

Immobilization alters *Rg*DAAO substrate specificity To identify *Rg*DAAO's most electrochemically active substrates, four different amino acids (D-serine, D-alanine, D-aspartate, and glycine) were tested with *Rg*DAAO$_{free}$. Chronoamperometric measurements monitoring the current profile from the incubation of *Rg*DAAO$_{free}$ in 100 μM of each substrate were performed. The steady-state current responses demonstrated that D-serine and D-alanine were the preferred substrates of *Rg*DAAO (ESM Fig. S4). Accordingly, D-serine and D-alanine were tested with both *Rg*DAAO$_{free}$ and *Rg*DAAO$_{immob}$ using spectrophotometry and electrochemistry, respectively. The spectrophotometric and electrochemical measurements were used to quantify concentration-dependent D-alanine:D-serine specific activity ratios (Fig. 4A & B). The ratios allow to evaluate the effect of enzyme immobilization on enzyme selectivity.

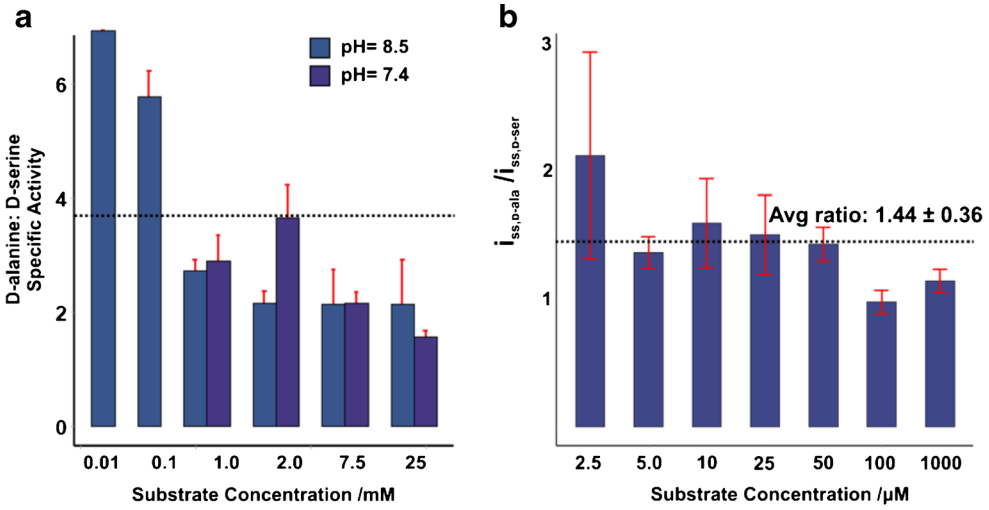

Fig. 4 **a** The specific activity of *Rg*DAAO was measured at various concentrations of D-alanine and D-serine individually using the *o*-DNS assay in NaPPi buffer (pH = 8.5) and KPi buffer (pH = 7.4). The specific activity at each concentration was used to calculate the D-alanine:D-serine specific activity ratio of *Rg*DAAO$_{free}$. Each bar shows the average specificity ratio of three ratios derived from measurements for each concentration. **B**) Ratio of biosensor response (i_{ss}) at various concentrations towards D-ala and D-ser ($n = 3$). Error bars represent ±SD. The biosensor steady state response was not measured at higher substrate concentrations due to a substrate inhibition effect masking i_{ss}

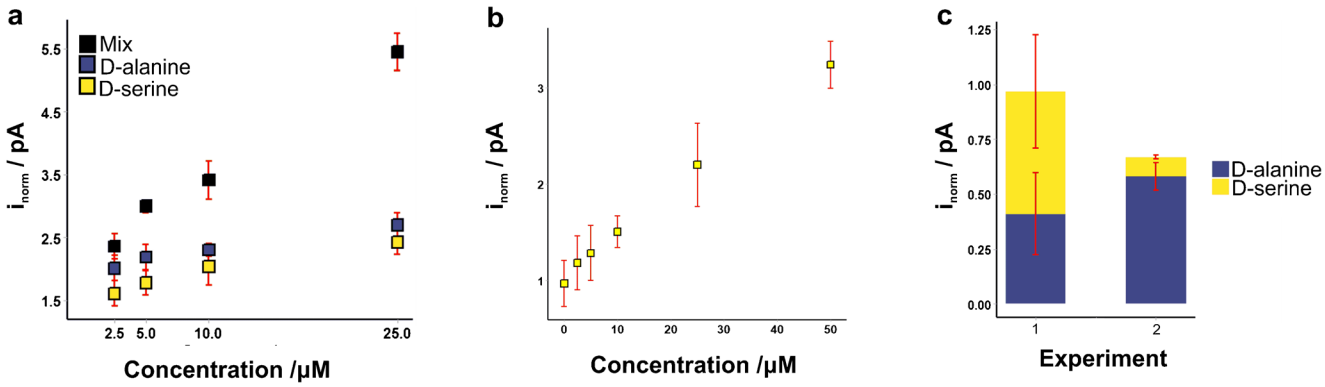

Fig. 5 *Rg*DAAO$_{immob}$ production of H_2O_2 from various substrate conditions. **a** Biosensor steady-state currents ($n = 3 \pm$ S.D.) for standard solutions of D-serine (yellow), D-alanine (navy), and equimolar D-serine/D-alanine mixtures (black) in PBS (pH = 7.4). **b** The steady-state current measured with the biosensor immersed in a solution of 0–25 μM D-serine, combined with 2.5 μM D-alanine ($n = 3 \pm$ S.E.M). The response increases linearly despite the presence of 2.5 μM D-alanine. **c** Effect of adding equimolar amounts (2.5 μM) of one D-amino acid to a solution containing the other on the oxidative steady-state current. The average of three measurements is shown ±S.D. The current is normalized to remove the capacitive contribution from the PBS buffer

For *Rg*DAAO$_{free}$, *Rg*DAAO is generally more selective towards D-alanine (Fig. 4a). Moreover, the *Rg*DAAO$_{free}$ specific activity ratios highlighted two main points: the ratios are on average ≥2 and the ratio increases drastically below 7.5 mM substrate concentration. Taken together, the results emphasize that the enzyme specificity depends on substrate concentration in the biosensor linear range. Additionally, a pH change has no significant effect on *Rg*DAAO specificity ratio (Fig. 4a) as confirmed with a Welch's *t*-test (for specific activity ratio values at pH 7.4 and 8.5, $t_{calc} = 0.5774 < t_{critical} = 3.182$). In contrast to *Rg*DAAO$_{free}$, the average *Rg*DAAO$_{immob}$ D-alanine/D-serine specificity ratio is <2 (Fig. 4b). While for both enzyme forms there is preferential selectivity of D-alanine over D-serine, enzyme immobilization results in a lower dependence on the substrate concentration, apparently increasing *Rg*DAAO selectivity towards D-serine.

Dual substrate presence does not always prevent single substrate detection with *Rg*DAAO$_{immob}$ Typically, a single amino acid is probed with biosensors and the presence of unwanted amino acids interferes with biosensor responses [68–70]. To explore the extent of the interference effect, the *Rg*DAAO biosensor was calibrated in standard D-serine (2.5–25 μM) (Fig. 5a, yellow), D-alanine (Fig. 5a, navy), and equimolar D-serine and D-alanine solutions (Fig. 5a, black).

Using chronoamperometry, the i_{ss} for D-serine and D-alanine mixtures was larger than that for pure D-alanine and D-serine solutions. For example, a mixture of 2.5 μM D-serine and 2.5 μM D-alanine generates an $i_{ss} = 3$ pA, compared to an $i_{ss} < 2.5$ pA for pure solutions of 5 μM D-alanine or D-serine. The i_{ss} increase is attributed to substrate specific reaction velocity (SEA) with *Rg*DAAO [71]. The results suggest that both amino acids are depleted by *Rg*DAAO, resulting in increased H_2O_2 production and making it challenging to attribute the biosensor response to a single D-amino acid. Consequently, in conditions where D-serine and D-alanine co-localize, such as the plasma and the pituitary gland, the biosensor may not accurately quantify a single D-amino acid.

Nonetheless, D-serine may still be quantified in the presence of constant D-alanine levels as evidenced by the linear current increase in standard D-serine solutions (Fig. 5b). Indeed, most biological environments do not have constant or equimolar concentrations of D-alanine and D-serine and the level of one or both D-amino acids may change following a release process. To simulate time-dependent release, D-serine and D-alanine were added sequentially instead of simultaneously. The addition of D-alanine to a D-serine solution increased the i_{ss} by more than 100% whereas the addition of D-serine to a D-alanine solution increased the i_{ss} by less than 20% (Fig. 5c), allowing a valid evaluation of D-serine level changes. Hence, constant D-alanine levels enable quantification of D-serine level changes. Conversely, time-dependent release of both D-serine and D-alanine do not allow individual D-amino acid quantification.

Conclusions

We report an analytical method (MECA) to characterize the kinetics of H_2O_2 production from free and immobilized enzymes using PPD-modified MEs. Using *Rg*DAAO for proof of concept, we validated the MECA by comparing K_m values for *Rg*DAAO$_{free}$ determined by a spectrophotometric assay, the Shu and Wilson method, and the MECA method. The MECA method enabled us to study enzyme selectivity differences between free and immobilized *Rg*DAAO forms. As

such, the MECA is a useful tool for the characterization of other non-redox enzymatic biosensors that rely on quantification of electrochemical products.

The development of such biosensors often employs glutaraldehyde cross-linking of *Rg*DAAO to a modified electrode surface [36, 38]. To assess alternative safe and sustainable cross-linkers such as poly(ethylene glycol) diglycidyl ether (PEDGE) [23], the MECA is used to extract generalized assessment metrics for various enzymatic biosensor architectures. Thus, the MECA could be useful to address questions concerning the cross-linking and cross-linker efficiency and their effect on enzyme activity.

We also demonstrate that substrate concentration modifies enzyme selectivity for free and immobilized *Rg*DAAO: modifications in enzyme selectivity are advantageous for biosensor application in selective analyte measurements. The effect of an unwanted D-alanine presence on D-serine quantification was also evaluated showing that under fixed D-alanine levels, biosensors remain useful for D-serine quantification.

Increasing the pool of methods to characterize immobilized enzymes on solid supports is beneficial to wide a range of fields, most prominently for biofuel cell and biosensor design. Future extensions to this work include exploring alternative cross-linker methodologies and the use of variant enzymes with altered substrate selectivity for improved accuracy in quantitative D-amino acid in situ measurements.

Supplementary Information The online version contains supplementary material available at https://doi.org/10.1007/s00216-021-03273-z.

Data transparency All data is available from the authors upon reasonable request.

Author contributions The manuscript was written through the contributions of all authors.

Funding S.M. and J.M. received financial support from the Natural Sciences and Engineering Research Council of Canada (NSERC) and MITACS. LP was supported by Fondo di Ateneo per la Ricerca.

Declarations

Conflict of interest The authors declare no competing interests.

References

1. Ehret F, Wu H, Alexander SC, Devaraj NK. Electrochemical control of rapid bioorthogonal tetrazine ligations for selective functionalization of microelectrodes. J Am Chem Soc. 2015;137:13.
2. Schneider E, Clark DS. Cytochrome P450 (CYP) enzymes and the development of CYP biosensors. Biosens Bioelectron. 2013;39(1):1–13.
3. Tak-Shing Ching C, Chang J-W, Sun T-P, Shieh H-L, Tsai C-L, Huang H-W, et al. An amperometric biosensor array for precise determination of homocysteine. Sensors Actuators B. 2010;152:94–8.
4. Li Z, Yu Y, Li Z, Wu T, Yin J. The art of signal transforming: electrodes and their smart applications in electrochemical sensing. Anal Methods. 2015;7:9732.
5. Feng W, Ji P. Enzymes immobilized on carbon nanotubes. Biotechnol Adv. 2011;29(6):889–95.
6. Pundir CS, Lata S, Narwal V. Biosensors for determination of D and L-amino acids: a review. Biosens Bioelectron. 2018;117:373–84.
7. Vasylieva N, Barnych B, Meiller A, Maucler C, Pollegioni L, Lin J-S, et al. Covalent enzyme immobilization by poly(ethylene glycol) diglycidyl ether (PEGDE) for microelectrode biosensor preparation. Biosens Bioelectron. 2011;26:3993–4000.
8. Andler SM, Goddard JM. Transforming food waste: how immobilized enzymes can valorize waste streams into revenue streams. npj Sci Food. 2018;2(1):19.
9. Rehm FBH, Chen S, Rehm BHA. Bioengineering toward direct production of immobilized enzymes: a paradigm shift in biocatalyst design. Bioengineered. 2018;9(1):6–11.
10. Neira HD, Herr AE. Kinetic analysis of enzymes immobilized in porous film arrays. Anal Chem. 2017;89(19):10311–20.
11. Bartlett PN, Cooper JM. A review of the immobilization of enzymes in electropolymerized films. J Electroanal Chem. 1993;362:1–12.
12. D'souza SF. Immobilization and Stabilization of biomaterials for biosensor applications. Appl Biochem Biotechnol. 2001;96.
13. Kim D, Herr AE. Protein immobilization techniques for microfluidic assays. Biomicrofluidics. 2013;7(4).
14. Marangoni AG. Immobilized enzymes. In: Enzyme kinetics. Hoboken, NJ, USA: John Wiley & Sons, Inc.; p. 116–20.
15. Anne A, Cambril E, Chovin A, Demaille C. Touching surface-attached molecules with a microelectrode: mapping the distribution of redox-labeled macromolecules by electrochemical-atomic force microscopy. Anal Chem. 2010;82(15):6353–62.
16. Jensen UB, Ferapontova EE, Sutherland DS. Quantifying protein adsorption and function at nanostructured materials: enzymatic activity of glucose oxidase at GLAD structured electrodes. 2012.
17. Bourdillon C, Demaille C, Moiroux J, Savéant J-M. Activation and diffusion in the kinetics of adsorption and molecular recognition on surfaces. Enzyme-amplified electrochemical approach to biorecognition dynamics illustrated by the binding of antibodies to immobilized antigens. P Curr Opin Biotechnol. 1998;70(7):2401–8.
18. Limoges B, Savéant J-M, Yazidi D. Quantitative analysis of catalysis and inhibition at horseradish peroxidase monolayers immobilized on an electrode surface. J Am Chem Soc. 2003;125(30):9192–203.
19. Limoges B, Marchal D, Mavré F, Savéant JM. Electrochemistry of immobilized redox enzymes: kinetic characteristics of NADH oxidation catalysis at diaphorase monolayers affinity immobilized on electrodes. J Am Chem Soc. 2006;128(6):2084–92.
20. Nguyen BH, Nguyen BT, Van Vu H, Van Nguyen C, Nguyen DT, Nguyen LT, et al. Development of label-free electrochemical lactose biosensor based on graphene/poly(1,5-diaminonaphthalene) film. Curr Appl Phys. 2016;16(2):135–40.
21. Polcari D, Perry SC, Pollegioni L, Geissler M, Mauzeroll J. Localized detection of d -serine by using an enzymatic amperometric biosensor and scanning electrochemical microscopy. ChemElectroChem. 2017;4(4):920–6.
22. Pribil MM, Cortés-Salazar F, Andreyev EA, Lesch A, Karyakina EE, Voronin OG, et al. Rapid optimization of a lactate biosensor design using soft probes scanning electrochemical microscopy. J Electroanal Chem. 2014;731:112–8.
23. Soldà A, Valenti G, Marcaccio M, Giorgio M, Pelicci PG, Paolucci F, et al. Glucose and lactate miniaturized biosensors for SECM-

based high-spatial resolution analysis: a comparative study. ACS Sensors. 2017.
24. Campos-Beltrán D, Konradsson-Geuken Å, Quintero JE, Marshall L. Amperometric self-referencing ceramic based microelectrode arrays for D-serine detection. Biosensors. 2018;8(1):28–34.
25. Sri Kaja B, Lumor S, Besong S, Taylor B, Ozbay G. Investigating enzyme activity of immobilized *Candida rugosa* lipase. J Food Qual. 2018;2018:1–9.
26. Baghayeri M, Zare EN, Lakouraj MM, Biosensor H, Fe N. A simple hydrogen peroxide biosensor based on a novel electro-magnetic poly(p-phenylenediamine)@Fe 3 O 4 nanocomposite. Biosens Bioelectron. 2014;55:259–65.
27. Moussa S, Mauzeroll J. Review—microelectrodes: an overview of probe development and bioelectrochemistry applications from 2013 to 2018. J Electrochem Soc. 2019;166(6):G25–38.
28. Ottone C, Romero O, Urrutia P, Bernal C, Illanes A, Wilson L. Enzyme biocatalysis and sustainability. In: Nanostructured catalysts for environmental applications. Springer International Publishing; 2021. p. 383–413.
29. Abolpour Homaei A, Sariri R, Vianello F, Stevanato R. Enzyme immobilization: an update. J Chem Biol. 2013.
30. Arabacı N, Karaytuğ T, Demirbas A, Ocsoy I, Katı A. Nanomaterials for enzyme immobilization. In: Green synthesis of nanomaterials for bioenergy applications. Wiley; 2020. p. 165–90.
31. Bolivar JM, Nidetzky B. On the relationship between structure and catalytic effectiveness in solid surface-immobilized enzymes: advances in methodology and the quest for a single-molecule perspective. Vol. 1868, Biochimica et Biophysica Acta - Proteins and Proteomics. Elsevier B.V.; 2020. p. 140333.
32. Bolivar JM, Schelch S, Mayr T, Nidetzky B. Mesoporous silica materials labeled for optical oxygen sensing and their application to development of a silica-supported oxidoreductase biocatalyst. ACS Catal. 2015;5(10):5984–93.
33. Grasso G, Fragai M, Rizzarelli E, Spoto G, Yeo KJ. A new methodology for monitoring the activity of cdMMP-12 anchored and freeze-dried on Au (111). J Am Soc Mass Spectrom. 2007;18(5):961–9.
34. Grasso G, D'agata R, Rizzarelli E, Spoto G, D'andrea L, Pedone C, et al. Activity of anchored human matrix metalloproteinase-1 catalytic domain on Au (111) surfaces monitored by ESI-MS †. J MASS Spectrom J Mass Spectrom. 2005;40:1565–71.
35. Meridor D, Gedanken A. Enhanced activity of immobilized pepsin nanoparticles coated on solid substrates compared to free pepsin. Enzym Microb Technol. 2014;67:67–76.
36. Zain ZM, O'Neill RD, Lowry JP, Pierce KW, Tricklebank M, Dewa A, et al. Development of an implantable d-serine biosensor for in vivo monitoring using mammalian d-amino acid oxidase on a poly (o-phenylenediamine) and Nafion-modified platinum-iridium disk electrode. Biosens Bioelectron. 2010;25(6):1454–9.
37. Maucler C, Pernot P, Vasylieva N, Pollegioni L, Marinesco SS. In vivo D-serine hetero-exchange through alanine-serine-cysteine (ASC) transporters detected by microelectrode biosensors. ACS Chem Neurosci. 2013;4:51.
38. Zain ZM, Ghani SA, O'Neill RD. Amperometric microbiosensor as an alternative tool for investigation of D-serine in brain. Amino Acids. 2012;43(5):1887–94.
39. Papouin T, Haydon P. D-serine measurements in brain slices or other tissue explants. Bio-Protocol. 2018;8(2).
40. Pollegioni L, Piubelli L, Sacchi S, Molla G. Review Physiological functions of D-amino acid oxidases: from yeast to humans.
41. MacKay MAB, Kravtsenyuk M, Thomas R, Mitchell ND, Dursun SM, Baker GB. D-serine: potential therapeutic agent and/or biomarker in schizophrenia and depression? Vol. 10, Frontiers in Psychiatry. Frontiers Media S.A.; 2019.
42. Sacchi S. d-Serine metabolism: new insights into the modulation of d-amino acid oxidase activity. 1551.
43. Rosini E, D'Antona P, Pollegioni L. Biosensors for D-amino acids: detection methods and applications. Int J Mol Sci. 2020;21(13):4574.
44. Polcari D, Kwan A, Van Horn MR, Danis L, Pollegioni L, Ruthazer ES, et al. Disk-shaped amperometric enzymatic biosensor for in vivo detection of D-serine. Anal Chem. 2014;86(7):3501–7.
45. Moussa S, Van Horn M, Shah A, Pollegioni L, Thibodeaux C, Ruthazer E, et al. A miniaturized enzymatic biosensor for detection of sensory-evoked D-serine release in the brain. J Electrochem Soc. 2021.
46. Spehar-Délèze A-M, Anastasova S, Vadgama P. Electropolymerised phenolic films as internal barriers for oxidase enzyme biosensors. Electroanalysis. 2014;26(6):1335–44.
47. Bin HS, Wu GW, Deng HH, Liu AL, Lin XH, Xia XH, et al. Choline and acetylcholine detection based on peroxidase-like activity and protein antifouling property of platinum nanoparticles in bovine serum albumin scaffold. Biosens Bioelectron. 2014;62:331–6.
48. Cappelletti P, Piubelli L, Murtas G, Caldinelli L, Valentino M, Molla G, et al. Structure–function relationships in human d-amino acid oxidase variants corresponding to known SNPs. Biochim Biophys Acta - Proteins Proteomics. 2015;1854(9):1150–9.
49. Rosini E, Caldinelli L, Piubelli L. Assays of D-amino acid oxidase activity. Front Mol Biosci. 2018;4:102.
50. Caligiuri A, D'Arrigo P, Rosini E, Pedrocchi-Fantoni G, Tessaro D, Molla G, et al. Activity of yeast d-amino acid oxidase on aromatic unnatural amino acids. J Mol Catal B Enzym. 2008;50(2–4):93–8.
51. Danis L, Polcari D, Kwan A, Gateman SM, Mauzeroll J. Fabrication of carbon, gold, platinum, silver, and mercury ultramicroelectrodes with controlled geometry. Anal Chem. 2015;87(5):2565–9.
52. Kangas MJ, Burks RM, Atwater J, Lukowicz RM, Williams P, Holmes AE. Colorimetric sensor arrays for the detection and identification of chemical weapons and explosives. Vol. 47, Critical reviews in analytical chemistry. Taylor and Francis Ltd.; 2017. p. 138–53.
53. Bard AJ, Faulkner LR. Electrochemical methods: fundamentals and applications. Mol Biol. 2015;8:129–33.
54. Lefrou C, Cornut R. Analytical expressions for quantitative scanning electrochemical microscopy (SECM). ChemPhysChem. 2010;11(3):547–56.
55. Biemans EALM, Verhoeven-Duif NM, Gerrits J, Claassen JAHR, Kuiperij HB, Verbeek MM. CSF d-serine concentrations are similar in Alzheimer's disease, other dementias, and elderly controls. Neurobiol Aging. 2016;42:213–6.
56. Kumashiro S, Hashimoto A, Nishikawa T. Free d-serine in postmortem brains and spinal cords of individuals with and without neuropsychiatric diseases. Brain Res. 1995;681(1–2):117–25.
57. Dos Santos JCS, Rueda N, Torres R, Barbosa O, Gonçalves LRB, Fernandez-Lafuente R. Evaluation of divinylsulfone activated agarose to immobilize lipases and to tune their catalytic properties. Process Biochem. 2015;50(6):918–27.
58. Coscolín C, Beloqui A, Martínez-Martínez M, Bargiela R, Santiago G, Blanco RM, et al. Controlled manipulation of enzyme specificity through immobilization-induced flexibility constraints. Appl Catal A Gen. 2018;565:59–67.
59. Barbosa O, Torres R, Ortiz C, Berenguer-Murcia Á, Rodrigues RC, Fernandez-Lafuente R. Heterofunctional supports in enzyme immobilization: From traditional immobilization protocols to opportunities in tuning enzyme properties. Biomacromolecules. 2013;14:2433–62.
60. Shu FR, Wilson GS. Rotating ring-disk enzyme electrode for surface catalysis studies. Anal Chem. 1976;48(12):1679–86.
61. Gonzalez-Navarro FF, Stilianova-Stoytcheva M, Renteria-Gutierrez L, Belanche-Muñoz LA, Flores-Rios BL, Ibarra-Esquer JE. Glucose oxidase biosensor modeling and predictors

optimization by machine learning methods. Sensors (Switzerland). 2016;16(11):16–22.
62. Fortier G, Brassard E, Bélanger D. Optimization of a polypyrrole glucose oxidase biosensor. Biosens Bioelectron. 1990;5(6):473–90.
63. Li J, Xiao L-T, Liu X-M, Zeng G-M, Huang G-H, Shen G-L, et al. Amperometric biosensor with HRP immobilized on a sandwiched nano-Au / polymerized m-phenylenediamine film and ferrocene mediator. Anal Bioanal Chem. 2003;376(6):902–7.
64. Shoja Y, Rafati AA, Ghodsi J. Enzymatic biosensor based on entrapment of d -amino acid oxidase on gold nanofilm/MWCNTs nanocomposite modified glassy carbon electrode by sol-gel network: analytical applications for d -alanine in human serum. Enzym Microb Technol. 2017;100:20–7.
65. Kornienko N, Ly KH, Robinson WE, Heidary N, Zhang JZ, Reisner E. Advancing techniques for investigating the enzyme–electrode interface. Acc Chem Res. 2019;acs.accounts.9b00087.
66. Kueng A, Kranz C, Lugstein A, Bertagnolli E, Mizaikoff B. Integrated AFM–SECM in tapping mode: simultaneous topographical and electrochemical imaging of enzyme activity. Angew Chem Int Ed. 2003;42(28):3238–40.
67. Baleizão C, Berberan-Santos MN. Enzyme kinetics with a twist. J Math Chem. 2011;49:1949–60.
68. Cordeiro CA, De Vries MG, Cremers TIFH, Westerink BHC. The role of surface availability in membrane-induced selectivity for amperometric enzyme-based biosensors. Sensors Actuators B Chem. 2016;223:679–88.
69. Weltin A, Kieninger J, Enderle B, Gellner A-K, Fritsch B, Urban GA. Polymer-based, flexible glutamate and lactate microsensors for in vivo applications. Biosens Bioelectron. 2014;61:192–9.
70. Lata S, Pundir CS. Fabrication of an amperometric D-amino acid biosensor based on nickel hexacyanoferrate polypyrrole hybrid film deposited on glassy carbon electrode..
71. Kaki SS, Adlercreutz P. Quantitative analysis of enzymatic fractionation of multiple substrate mixtures. Biotechnol Bioeng. 2013;110:78–86.